Structure-dependent electrical conductivity of protein: its differences between alpha-domain and beta-domain structures

X Y Zhang[1,2,5]**, Jian Shao**[1,2]**, S X Jiang**[1,2,4]**, Biao Wang**[1,5] **and Yue Zheng**[1,2,3]

[1] State Key Laboratory of Optoelectronic Materials and Technologies/Institute of Optoelectronic and Functional Composite Materials, Sun Yat-sen University, Guangzhou, 510275, People's Republic of China
[2] Micro&Nano Physics and Mechanics Research Laboratory, School of Physic and Engineering, Sun Yat-sen University, Guangzhou, 510275, People's Republic of China
[3] Departments of Mechanical Engineering and Civil and Environmental Engineering, Northwestern University, Evanston, IL 60208, USA
[4] School of Physics, Peking University, Beijing, 100871, People's Republic of China
[5] Sino-French Institute of Nuclear Engineering and Technology, Sun Yat-sen University, Zhuhai, 519082, China

E-mail: zhengy35@mail.sysu.edu.cn, yue.zheng@northwestern.edu and wangbiao@mail.sysu.edu.cn

Abstract

Electron transports in the α-domain and β-domain of proteins have been comprehensively investigated. The structure-dependent electron transport of proteins has been experimentally measured and theoretically simulated, and both the theoretical and experimental results demonstrate significant differences in electrical conductivity between the α-domain and β-domain. By controlling the feedback system of the scanning tunneling microscope (STM), the conductance of a single α-domain protein hemoglobin (Hgb) and a β-domain protein superoxide dismutase enzyme (SOD) were measured, respectively. The current signal of Hgb is obviously stronger, indicating that the α-domain is more conductive. To confirm our finding, molecular orbitals of both the β-domain in SOD and α-domain in Hgb have been analyzed based on first-principles calculations. As expected, tunneling transport and hopping in the α-domain are both more efficient, indicating that it is easier for electrons to transport through the α-domain, which are in great agreement with our experimental data. In order to explain our results, molecular structures of α- and β-domains have been carefully analyzed and show that the explanation should lie in the differences in packing mode between the α-domain and β-domain. This research should be very important to application prospects in molecular electronics.

S Online supplementary data available from stacks.iop.org/NANO/26/125702/mmedia

Keywords: molecular electronics, protein, conductance

(Some figures may appear in colour only in the online journal)

1. Introduction

Miniaturization of electronic devices has been improving our lives since the middle of the last century, and nowadays, the limit is approaching the nanoscale. For further downsizing, scientists are paying growing attention to the idea of integrating individual molecules to fabricate nanoscale electronic devices [1–3]. Now, it is known that the key issue in building molecular devices requires an in-depth understanding of electron transport properties of individual molecules. On this basis, it is possible to design nano-electronic components with desirable functions in the molecular scale

such as molecular switches, bio-rectifiers and bio-transistors [4, 5], etc. Among the numerous biomolecules, proteins are often considered as the most promising candidates because they are known to act as the materials for bioelectronics and play a crucial role in electron transfer processes in living creatures [6]. These include many vital processes related to energy conversion such as adenosine triphosphate production, photosynthesis and metabolism [7]. Comprehensive understanding of electron transport in proteins enables us to create higher electrical functionality through molecular design. The knowledge might also enable further research for relative diseases such as mitochondrial disease and the development of molecular bio-sensors [8–10]. Therefore, electron transport properties in proteins have attracted great interest in fields of bio-medicine, bio-engineering and bio-molecular electronics, etc.

Early studies on electron transport in proteins began with peptides, which are often considered as the segments of protein with relatively simple configurations. Theoretically, by establishing a model, such as the pathway model, the electron transport in peptides has been proved to be obviously dependent on bonds contacts and the composition of the coupling medium [11, 12]. These two factors are closely related to the molecular structure; thus, the configuration of the peptide was considered to be critical to its conductance [13, 14]. As for experimental approaches [15–19], the scanning tunneling microscope break junction (STM-BJ) approach [20, 21] and STM-I(t) measurement [22, 23] are both great techniques for measuring single molecule conductance. On the basis of abundant investigations, it has been verified that molecular structure is significant to electron transport in peptides. Typical work, such as the work of Nichols *et al* [24], have found that the conductance of peptide sequence $H(EL)_5C$ decreases dramatically when its molecular conformation is changed due to pH alteration. The structure of protein is usually more complicated than that of a peptide because the former can be considered as a combination of the latter. This complexity should result in stronger structural dependence of conductance and might make electron transport in proteins more controllable, which is highly desirable for developing molecular devices. Several phenomena have been found to reveal the structural dependence of protein conductance. For examples, Eduardo *et al* [25] have investigated the orientation-dependent electron transport in single proteins and shown that an electron transfer protein engineered to bind gold surfaces can be controllably oriented to tune the conductance of a single protein junction. Until now, one challenge in studying the conductivity difference between different types of domains is that the existing techniques for single molecule conductance measurement, such as STM-BJ and STM-I(t), are not fully suitable for measuring electron transport in proteins. Consequently, there is urgent need to develop an experimental method to measure the conductance of single proteins. The research of structural dependence of electron transport in proteins is just beginning. One of the most important subjects is the conductivity difference

between different types of structural domains in proteins, which still has not been thoroughly studied. Structural domains are the basic functional units in protein [26, 27]. Clarifying the conductivity differences between different types of domains enable people to reveal the principium of how proteins transfer electrons in nature and which structure dominants the electron transport in proteins.

In order to study the structure-dependent electrical conductivity of proteins, we want to measure and analyze the electrical conductivities of the α-domain and β-domain, which are mainly formed by α-helices or β-sheets, respectively. To achieve these, the conductance of two metalloproteins, i.e. hemoglobin (Hgb) and superoxide dismutase (SOD) (see supporting file figure S1), will be firstly measured. The reasons for choosing these two proteins as materials are given as follows: Hgb has a quaternary structure characteristic of globular proteins in which most of the amino acids form α-helices and make the protein consist of a globin domain. The globin domain is the most important α structure, which has been found in a large group of proteins, including transport proteins. The structural feature of globin is the same as most other α-domains, which involve fitting ridges of side chains along one α-helix into grooves between side chains of another helix to form a hydrophobic core. So, generally speaking, globin is the most representative α-domain. In contrast, most of the amino acids in SOD proteins form β-sheets and make the protein consist of an 8-stranded 'Greek key' beta-barrel domain. β-sheets have the usual twist, and when several such twisted sheets are packed together, they mostly form a barrel-like structure except for some rare cases in RNA viruses. Therefore, the beta-barrel domain is the most typical β-domain. Because a globin domain consists of 8 helices, and considering the comparability in size and topological features, the 8-stranded 'Greek key' beta-barrel in SOD is the most suitable sample representing the β-domain [26]. In addition, it is well known that proteins consist of the same kind of domain and have a similar structure even though they vary in amino acid sequence. In a crowd of candidates that consist of the chosen domains, Hgb and SOD are both well defined and have been intently studied. Therefore, Hgb and SOD are suitable and representative samples for comparing the conductivity of the α-domain and β-domain. In this paper, the feedback system of STM was carefully controlled in order to measure the conductance of the single protein. By obtaining the conductance of Hgb and SOD using STM, the differences in electron transport between them can be distinguished. Experimental results present abundant current data under different voltages without applying force on proteins and show significant differences of the conductivity between the α-domain and β-domain of proteins. In order to confirm the experimental finding, molecular orbitals of both the β-domain in SOD and α-domain in Hgb have also been simulated using the first-principles calculation. The hopping rate and tunneling transport of electrons in both the α-domain and β-domain have been analyzed to reasonably reveal the mechanism.
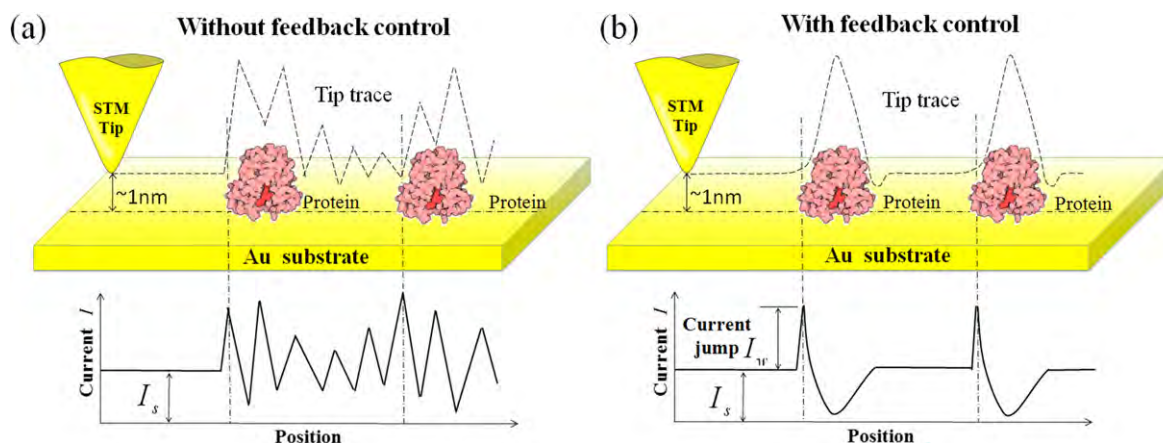
Figure 1. Schematic diagram of measuring the conductance of a single protein. Samples are sparsely placed on an atomic flat conductive substrate. When performing STM scanning, the tip is able to contact the protein naturally and measure the current signals. However, in (a) STM scanning with both proportional gain and integral gain, without controlling the feedback system, scanning trajectory of the STM tip over the substrate is sawtooth-like. Because the tunneling current is very sensitive to the distance between the STM tip and sample, the current signal of protein will be buried. (b) STM scanning with only proportional gain. By controlling the feedback system and eliminating proportional gain, the scanning trajectory of the STM tip is smoothed so that the current signal of the single protein is identifiable.

2. Experimental details

2.1. Materials

The purchased Hgb (from swine, Sigma-Aldrich) and SOD (from human, Nuptec) are in the form of lyophilized powder. To achieve the low density of proteins coverage on the substrate for conductance measurement, the lyophilized powders were first dissolved in ultra-pure water with the appropriate concentration, respectively. The solutions were then incubated for 2 h. Later, 2 ml of the solution were dropped on an atomically flat Au film supported by a mica substrate (SPI Supplies and Structure Probe, Inc.), which had been flame annealed right before use. After the proteins were absorbed on the substrate spontaneously, the samples were rinsed and blown dry by pure nitrogen.

2.2. STM method for measuring conductance of the single protein

In this work, we did not use the existing techniques for single molecule conductance measurements, such as STM-BJ and STM-*I*(t), because these techniques are not fully suitable for measuring electron transport in protein. In STM-BJ, the current signals are obtained when the molecule is under stretching, which has been reported to be influential to the molecule's conductance [27]. Because the structure of protein is much more sensitive to mechanical force than simple molecules, such as alkanedithiols, the deformation of protein in STM-BJ might seriously affect the test results. In the STM-*I*(t) measurement, the sample molecule should be much smaller than the gap between the STM tip and substrate so that the attachment and detachment between the molecule and STM tip can be identified. Since proteins are normally larger than the gap, the STM tip might come into contact with protein before any through-space tunneling current can be observed, causing it to be difficult to measure protein

conductance through the STM-*I*(t) measurement. Instead of the STM-BJ and STM-*I*(t) measurement methods, the conductance of a single protein in this work was measured under the STM constant current mode with controlled feedback system. By means of our method, the conductance of a single protein can be measured without the stretching. The basic idea of this approach is illustrated in figure 1. In constant current mode, by means of a carefully controlled feedback system, the conductance of a single protein on Au film is characterized directly during STM scanning. In detail, because the size of protein is normally larger than the gap between the STM tip and conductive substrate, the attachment between the STM tip and protein can be naturally achieved during the scanning. When the tip comes into contact with protein, the total current detected by STM consists of two parts, which are the through-space tunneling current I_t and the current through the protein I_w [22]. However, I_w is normally not identifiable in ordinary STM constant current mode. As the STM tip scans across the sample, under the influence of the feedback system, the STM tip would either uplift or decline for a small distance in each scanning step, making the trace of the STM tip like a sawtooth, as shown in figure 1(a). Because the through-space tunneling current is very sensitive to the distance between the conductivity substrate and the tip [28, 29], the sawtooth-like trace will induce current fluctuations (figure 1(a)), which can easily bury the current signals of proteins. This problem can be overcome by a thorough analyzation of the feedback system, which is described as $u = \gamma (I - I_s) + \eta \int_0^t (I - I_s) dt$ [29]. u represents the uplifting distance of the tip. I is the total current that is detected by STM. I_s is the set point current. t represents the span of time, while I does not equal I_s; it will be reset to zero at each time $I - I_s = 0$. γ and η are parameters that are related to the feedback sensitivity. From the feedback equation, it can be found that the sawtooth-like trace of the STM tip is caused by the proportional gain (i.e. the first term in the equation).

Accordingly, to eliminate the current fluctuations, we shut down proportional gain but maintain the integral gain in the operation to protect the tip from crushing during the scanning. On this basis, together with the appropriate scanning rate and integral gain sensitivity, we managed to make the tip scan over the substrate at a steady height and with a smooth trace, as illumined in figure 1(b). On this basis, current fluctuations can be greatly reduced, making the current signal of the protein especially identifiable and appear to be the 'current jump' (figure 1(b)). Also, the through-space tunneling current I_t is equal to the set point current I_s. Thus, the current through the proteins can be calculated as $I_w = I - I_s$. To differentiate the former two typical measurement methods, such as STM-BJ and STM-*I*(t), our improved method in this work is named the STM-HA (i.e. Horizontal Approaching) measurement method.

Our method stabilizes the through-space tunneling current and enhances the information of the current image in constant current mode by controlling the feedback system. As such, the current signals of proteins can be precisely extracted. Compared with previous techniques for measuring conductance of a single protein, our methods have two advantages. First, the attachment of the STM tip and protein is naturally achieved during scanning. Thereby, the current signal of a single protein is obtained before any force is applied on the protein, which avoids the influence of force on the protein structure. Second, the measurements are performed automatically in the process of STM scanning. Thus, sufficient data can be conveniently obtained from this very efficient experimental approach. Compared with the constant height mode, this approach provides more protection to the tip; thus, the scanning area is much larger. This is very important because in studying the conductance of molecules, one needs to obtain enough data for statistical analysis. In addition, because the integral gain is still functional during the scanning, the tip will rise right after it comes into contact with the proteins (figure 1(b)), which reduces the contact time between the tip and molecules. Thus, the tip is rarely terminated by molecules in our methods. Even if the tip is terminated by molecules, because the size of proteins in our work is larger than the gap between the tip and substrate, the tunneling current will be seriously disturbed. In this case, the current image will be messy and easily identified. Naturally, the data under this situation will be rejected. It should also be noticed that due to the slow gain, all adsorbates and morphologies can result in a similar current jump in our technique. In the current image, the current change will show the outline of every bulge on the substrate. Therefore, the flatness of the substrate and purity of the sample are very important to the validity of the data. For an atomically flat Au substrate, the bulge is normally much larger than the size of the protein; the current change induced by the morphology will appear to be lines in the current image. In contrast, the current changes induced by proteins appear to be dots, making it easy to identify whether the signal comes from protein. The reliability of our approach has been verified by measuring the conductance of a single alkanedithiols molecule, the results of which are in great agreement with that in

the previous article [23] (see supporting file figure S2). CSPM 5500 (Being Co. Ltd) was used to perform the STM scanning. The setpoint current was 0.4 nA, and the typical scanning rate was 0.6 Hz. The STM Au tips in the measurement were prepared using 0.25 mm diameter gold wire by electrochemical etching [30] (see supporting file figure S3). The STM scans were performed under room temperature at about 23 °C and ambient pressure. The humidity of the environment was about 40%. The setpoint current was set to be 0.4–0.8 nA during the scanning. For a 200 nm × 200 nm scan scope, the scan rate was set to be 0.6–0.8 Hz. According to our experience, if the scan speed is slower, wavy noise might appear in the current image. On the other hand, if the scan is too fast, the tip might crash into the substrate. Moreover, all the current changes induced by proteins or the morphology of the substrate will be followed by a long black line, which make the data hard to analyze.

2.3. Obtaining the molecular orbitals via first-principles calculation

We also investigate the orbitals of the proteins via first-principles calculations to study the structure-dependent electrical conductivity of protein. Configurations of both SOD and human Hgb are imported from PDB, the PDB-IDs of which are 2SOD and 1HHO, respectively. To implement first-principles calculations efficiently, we 'cut off' from SOD the amino acid residue (AA) 3-34, which consists of three *β*-strands linked by a bend, a beta bridge and a turn; the rest of the SOD was discarded. In the same way, the AA 101-141, which consists of two *α*-helices linked by a 3_{10}-helix, are cut off from the beta chain of Hgb (see supporting file figure S4). The 'cut-off' parts of proteins were used directly to obtain the molecular orbitals; no relaxation was performed before the calculations. All calculations are performed using generalized gradient approximation (GGA-PBE), implemented in Atomistix Toolkit (ATK). The double-*ζ* polarized basis set is used for all the atoms. The molecular orbitals are plotted in 0.02 isosurfaces, colored with a sign.

3. Results and discussions

3.1. Experimental results

Using the STM-HA method, the total currents at individual points of proteins-coated Au film were recorded to yield the current image. Typical results are shown in figure 2. In current images of bare Au film (figures 2(a), (b)), no current jump can be found. In contrast, a lot of white dots appear in the current images of Hgb-coated Au film (figures 2(c), (d)), which represent the current signals of the proteins. We have also analyzed the section lines of both current images. As shown in figure 2(e), several current jumps appear obviously in the current image of the sample with the proteins coated. Conversely, no current jump can be found in the section line of the bare substrate.
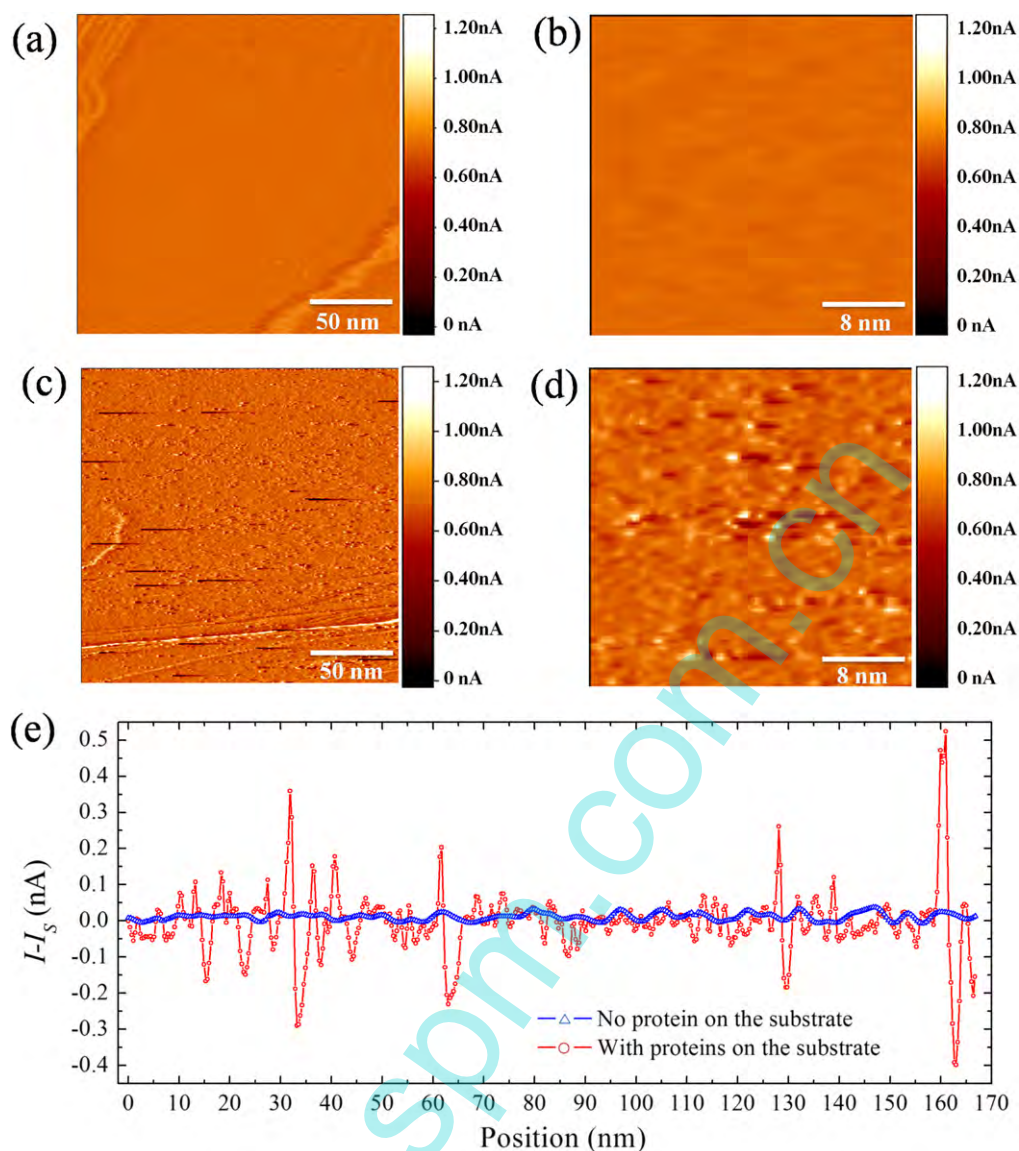
Figure 2. Experimental results from STM under tunneling voltage 0.4 V. (a) The current image of a bare Au substrate. It can be seen that the substrate is very clean and atomically flat. (b) The current image of a bare Au substrate with more details. (c) The current image of a Au substrate with proteins on its surface. Lots of white dots appear, which represent the current signals of proteins. (d) The current image of proteins included with the substrate with more details. (e) Section lines obtained from bare Au film and proteins coated Au film, respectively. Current jump can only be found in section lines of proteins coated Au film.

The correspondence between the change in total current and lifting of the STM tip around the current jump has also been checked, which is shown in figure 3(a). As we expected, at points i and iv, the STM tip is scanning on the Au substrate; thus, no obvious current change and tip uplifting can be observed (figure 3(b)). However, at point ii, the contact between the STM tip and protein gives rise to the current jump, which then leads to the lifting of the STM tip. At point iii, with further uplifting of the tip, the current rapidly decreases, making the current signal remarkably identifiable. In figure 3, the fluctuation is less than ±0.1 nm when the tip is scanning on the substrate. This result indicates that every time the STM tip comes into contact with the protein, the distance between the tip and substrate will almost be the same; the

deviation is less than 0.1 nm. This important feature ensures the repeatability and comparability of our measurement data.

The current signals of both Hgb and SOD under voltages from 0 V to 0.8 V have been analyzed by means of the STM-HA approach, the results of which are shown in figure 4. Under each voltage level, the differences between peak values of 150 current jumps of individual proteins and the set point current have been recorded to yield the histograms for Hgb and SOD, respectively (table S1). It can be seen that the current signals under each voltage level have a certain distribution. This is caused by the fact that we used native proteins in our measurements. The orientation of proteins and the contact with the STM tip are stochastic. Thus, the influences of the contact resistance and protein orientation on
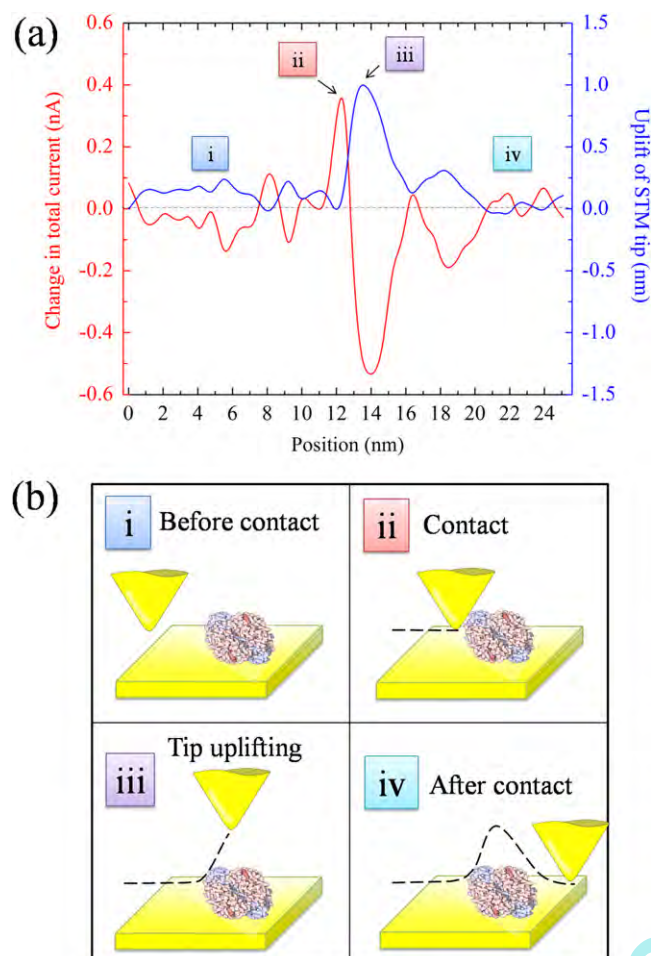
Figure 3. Schematic representation of the measure method. (a) The change in total current and rise of the STM tip around the current jump. (b) A schematic representation showing the proposed stages of attachment and detachment of the protein and STM tip.

electron transport are also reflected in the histogram. On the other hand, each histogram exhibits only one pronounced peak (figures 4(a), (b)). The current values of these peaks in the histogram are considered to be the characteristic current, which have been extracted to estimate the *I-V* curves of Hgb and SOD, as shown in figure 4(c). The results show that conductance in Hgb is better compared to SOD (also, see supporting file figure S5). The ratio of the conductance of Hgb and SOD is between 1.40 and 1.50 (figure 4(d)). When applying a voltage of 0.2 V, the current through Hgb is about 0.1 nA higher than that of SOD (figure 4(d)). This difference of the current increases with the increasing of the bias voltage and reaches 0.26 nA under 0.8 V. The significance of the difference in current between the two proteins under each voltage level has been verified by use of software package IBM SPSS Statistics. Statistical analysis has been performed by three methods, including the independent t-test, median test and Mann-Whitney U test. The results of all three tests consistently demonstrate that the conductances of the two proteins are significantly different from each other. The confidence level reaches 99.9%.

To compare the electron transport properties of the α-domain and β-domain, we further consider the size difference between Hgb and SOD. According to the etching method for producing the STM tip, the geometry of the tip is normally spherical or conical [30]. Therefore, when the current signal of the protein is being measured, the contact point between the protein and STM tip should be on the inclined plane of the tip, as illustrated in figures 4(e), (f). Because of the size difference between the two proteins, the distance between the electrodes in the Hgb case (figure 4(e)) should be longer compared to that in the SOD case (figure 4(f)), at least in statistical terms. According to experimental results, under the same voltage, the current signals of Hgb are stronger than signals of SOD even though the size of SOD is smaller, indicating that the conductivity of Hgb is better than that of SOD. Because these two proteins are mainly formed by an α-domain or β-domain, respectively, it can be qualitatively concluded that conductivity of the α-domain is higher than that of the β-domain. Our estimation also suggests that the conductivity of the α-domain should be 2 to 3 times higher than that of the β-domain. It should be pointed out that in the analysis of conductivity difference, it is assumed that the tip stay intact and not be terminated by proteins. As discussed before, if the tip is damaged or terminated by proteins, the current image will be messy, and the data should not be accepted.

3.2. First-principles simulations on molecular orbitals of an α-domain and β-domain

In order to confirm our experimental results and reveal the mechanism of the difference in electron transport between the α-domain and β-domain, we performed the first-principles calculation to study the electron transport in both Hgb and SOD, respectively. Instead of calculating the electronic conductance [31–34] of the α-domain and β-domain, we analyzed their molecular orbitals to distinguish between their electron transport differences. The reason is that the relaxation for introducing electrodes is too resource-consuming, making it very difficult to calculate the electronic conductance of a biomacromolecule via the first-principles calculation. Alternatively, the molecular orbital represent regions in the molecule in which an electron is likely to be found. By studying the morphology of the molecular orbital, the properties of electric transport in a single molecule can be qualitatively analyzed [35, 36]. With appropriate data from the protein data bank (PDB), the molecular orbital of a protein can be calculated self-consistently without any relaxation, which makes it feasible to study the electron transport of a single protein by calculating its molecular orbital through the first-principles calculation.
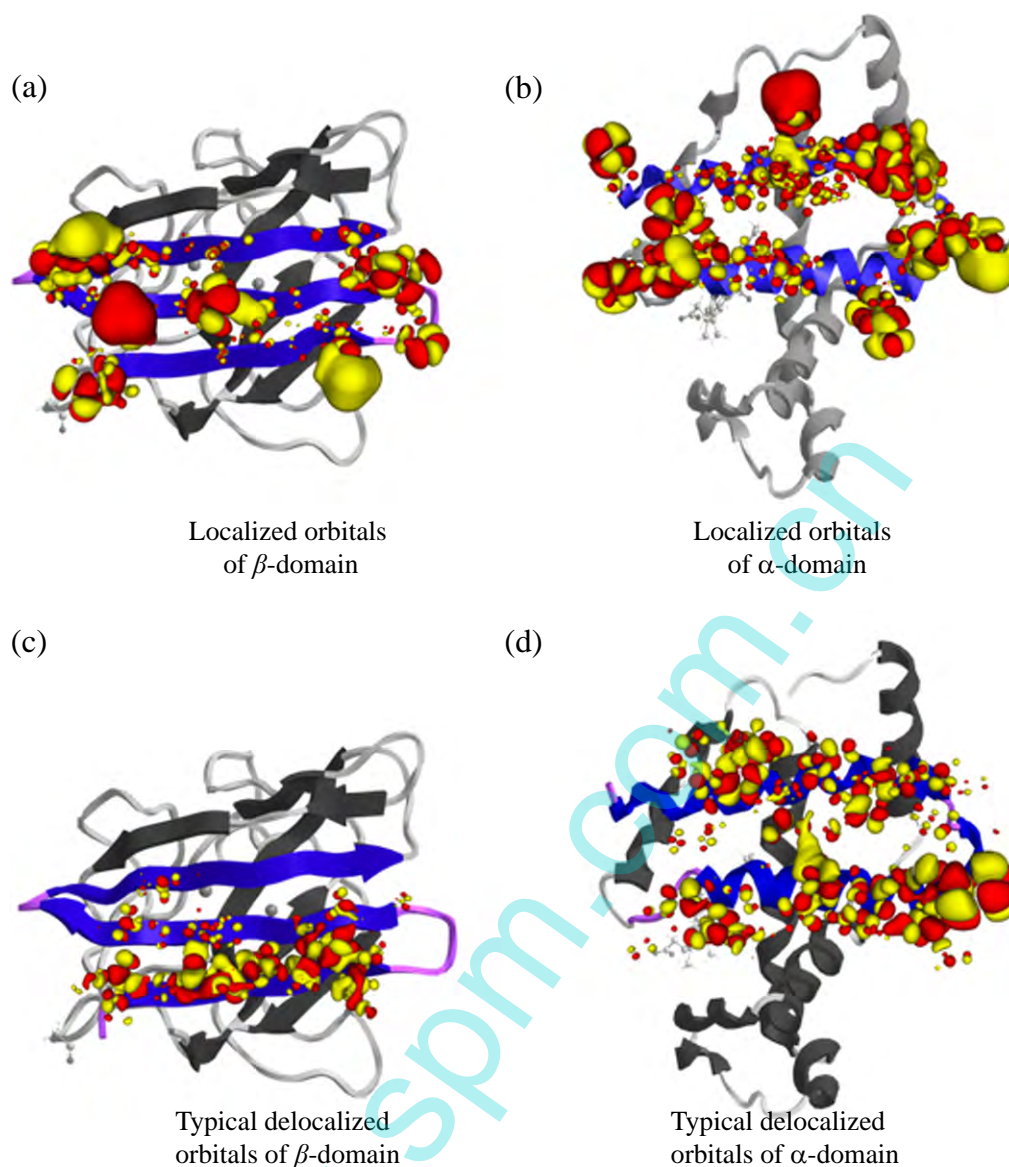
We calculated molecular orbitals of three β-strands in SOD and two α-helices in Hgb, respectively. The results show that the molecular orbitals of the α-domain and β-domain are obviously different (figure 5 and table 1). Indeed, there are two mechanisms that contribute to the electron transport in protein, which are hopping and tunneling transport [37, 38]. The hopping mechanism describes the transport lead by the
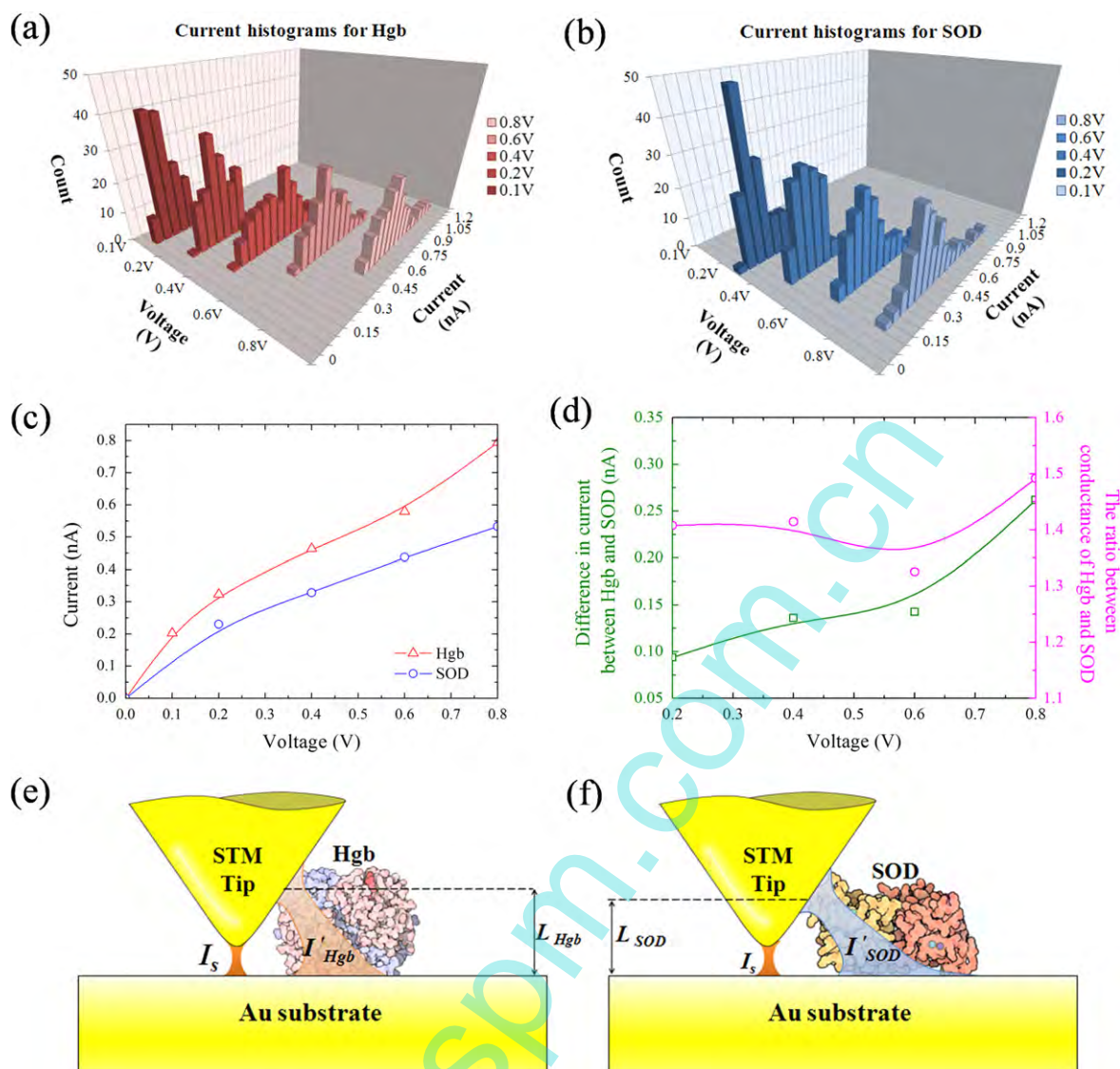
Figure 4. Electric current for different kinds of proteins. Histograms of current for both (a) Hgb (red) and (b) SOD (blue). A pronounced peak can be found in each histogram, from which the representative current under each voltage can be determined. (c) I-V curves for both Hgb (triangle) and SOD (square) under voltage from 0.1 V to 0.8 V. It is obvious that Hgb has better conductance than SOD. (d) Comparisons between currents of Hgb and SOD under each voltage level. (e), (f) Illumination of the attachment between the STM tip and protein when measuring the conductance of (e) Hgb and (f) SOD. The current that was sensed by the system should contain two parts: the tunneling current and current through the protein. The current jumps that appear in STM scanning should be the latter. Because of the cone-shape of the tip and the size difference between Hgb and SOD, the contact point between the STM tip and Hgb is higher than that of SOD.

jumping of electrons from one to another site with different energy levels. The relation between hopping and conductivity of a molecule can be described by hopping rate $f_{ij} = f_0 \exp(-\gamma r_{ij}) \exp(-\Delta E_{ij}/kT)$[39], where f_0 is the maximum hopping rate; γ is the inverse localization radius, which is relative to the delocalization of orbitals and states how well charge carriers can jump across the distance between site i and j; r_{ij} is the distance between i and j; and ΔE is the energy difference between initial state i and final state j. With the larger hopping rate, charge carriers are more likely to jump from one location to another, representing higher conductivity in the molecule. The hopping mechanism involves both delocalized and localized orbitals. Therefore, we analyzed

localized orbitals of both the α-domain and β-domain located inside the energy range of ± 0.7 eV near the Fermi level (see supporting file figure S6 and table S2). In our analysis, if one orbital encircles more than an entire α-helix or β-sheet, it is considered as a delocalized orbital. The results have been shown in figures 5(a), (b). It is obvious that the inverse localization radius and the density of orbitals are both higher in the α-domain. Also, there are 33 localized and delocalized orbitals in the α-domain compared to only 22 in the β-domain. Thus, it can be estimated that the mean energy difference between every jump of electron in the α-domain must be smaller. Overall, the hopping rate in the α-domain is higher than that in the β-domain, which indicates that the jumps of electrons from one location to another in the α-domain is

(a)

Localized orbitals
of β-domain

(b)

Localized orbitals
of α-domain

(c)

Typical delocalized
orbitals of β-domain

(d)

Typical delocalized
orbitals of α-domain

Figure 5. The first-principles calculation. (a) The superposition of 10 localized orbitals of the α-domain located inside the energy range of ±0.7 eV near the Fermi level. Two localized orbitals on the other side of the helices and 21 delocalized orbitals are not plotted. (b) The superposition of 8 localized orbitals of the β-domain located inside the energy range of ±0.7 eV near the Fermi level. Three localized orbitals on the other side of the sheet and 12 delocalized orbitals are not plotted. (c) A typical delocalized orbital of the β-domain located at 0.64 eV above the Fermi level. The orbital does not delocalize through the domain, indicating that the interaction between two nearby chains is weak (d) A typical delocalized orbital of the α-domain located at 0.66 eV above the Fermi level. The orbital is delocalized throughout the helices, indicating strong interaction between two nearby helices. Particularly, the wave function bridges through the two helices.

Table 1. The summarized results of the first-principles calculation for molecular orbitals of Hgb and SOD.

	Region of calculation	Delocalized orbitals		Localized orbitals		Total number of orbitals
		Count	delocalization	Count	Overlapping density	
Hgb	Two α-helices	21	High	12	High	33
SOD	Three β-chains	12	Low	11	Low	23
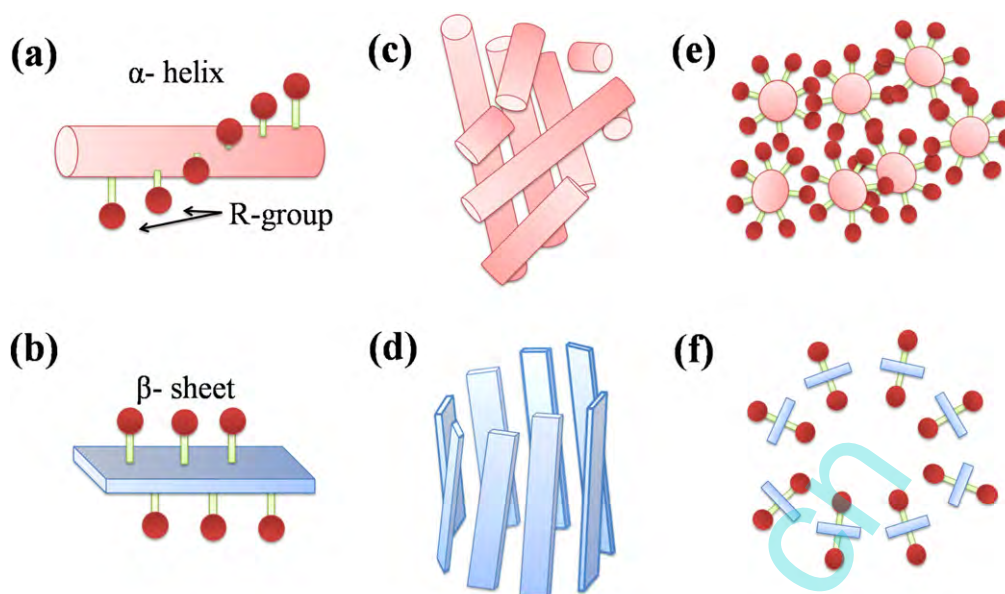
Figure 6. Discussions for differences between the Alpha-domain and Beta-domain structures. (a) R-groups trend to surround the α-helix. (b) Conversely, R-groups trend to point alternately above and below the β–sheet. (c) In a typical α-domain (Globins domain), there is no morphological constraint on α-helices when building the structure. (d) However, in a typical β-domain ('Greek key' beta-barrel), β–sheets (or β–strands) must be aligned adjacent to each other, which seriously limits the configuration of the β-domain. (e) The forming of the α-domain depends on the bonding of R-groups on α-helices, which makes the overlapping density of R-groups (ODR) in the α-domain high. (f) As a result of the limited configuration, the mean distance between R-groups is not as close as that in the α-domain. Therefore, the ODR in the β-domain is low.

easier than that in the β-domain. Because the number of jumping steps for electrons to transport through the molecule is related to the size of the molecule, it can be concluded that the conductivity of the α-domain is much better than that of the β-domain. According to previous articles, because the coherence length of the electron is normally much smaller than the size of the protein, the transport in proteins should mostly occur via the hopping mechanism. However, to ensure the integrity of our theory, the tunneling transport of both Hgb and SOD has also been analyzed as follows: In tunneling transport, electrons tunnel through the protein on certain delocalized orbitals near to the Fermi level. Therefore, delocalization of orbitals is essential to the efficiency of the tunneling transport. Typical conformations of the delocalized orbital near to the Fermi level of the α-domain in Hgb and the β-domain in SOD have been shown in figures 5(c), (d), respectively. It is shown that the orbital in the β-domain does not delocalize through the domain but is constrained in individual β-strands, indicating a low level of delocalization. In contrast, the orbitals in the α-domain are delocalized and extended to the whole domain. Therefore, with higher delocalization, the α-domain is more beneficial to the tunneling transport of electrons.

3.3. Structure-dependent conductivity of proteins

To reveal the mechanism of difference in transport between the α-domain and β-domain, the positioning of molecular orbitals in the two domains has been thoroughly analyzed (see supporting file, table S3), respectively. It is found that most localized orbitals in both the α-domain and β-domain are located around one or several adjacent R-groups. Consequently, the density of localized orbitals, which is critical to the hopping rate, is determined by the crowding level of R-groups and compactness of the protein. Because of the heliciform, the average distance between two adjacent R-groups in the α-helix is about 0.15 nm (figure 6(a)). In contrast, the β-sheets are in an almost fully extended conformation in which the distance between two adjacent R-groups is 0.32–0.34 nm [40] (figure (b)). Therefore, the crowding level of R-groups in the α-helix is higher. Moreover, the difference in packing mode between the typical α-domain (Globin domain) (figure 6(c)) and β-domain ('Greek key' beta-barrel) (figure 6(d)) further widens the gap. The phenomenon, as before, is the formation of the α-domain, which involves fitting ridges of R-groups along one α-helix into grooves between R-groups of another helix [26]. As such, the R-groups on distinct helices are closely packed together to form a hydrophobic core, as shown in figure 6(e). In contrast, the formation of the β-domain relies on hydrogen bonds between β-strands, leading to a loose configuration of R-groups (figure 6(f)). As a result, the compactness of the α-domain is much higher than that in the β-domain, making the density of localized orbitals in the α-domain higher. For delocalized orbitals, the most delocalized orbitals in the β-domain are found to be constrained in individual β-strands. However, delocalized orbitals in the α-domain can be bridged by certain R-groups of two helices and extend to the whole domain (figure 5(b)) (also see supporting file, figure S7), which is of great advantage to both tunneling and hopping. It is also found that all the bridges of molecular orbitals are present inside the hydrophobic core of the α-domain,

which proves the importance of the packing mode to electron transport.

In summary, the structure of the α-domain is more beneficial to electron transport. It should be pointed out that although the globin and beta-barrel we study in this work are both typical and representative domain structures, there still exists some infrequent α- or β-domains with different structural features. For example, neuraminidase domains in some RNA viruses do not form barrel structures. Moreover, the formation of a coiled-coil domain in fibrous proteins involves a 'knobs in holes' mode, which is slightly different from globin. The electron transport properties of these unfrequented α- or β-domains still need further investigation.

4. Conclusions

In this work, the electrical conductivity differences between the α-domain and β-domain have been investigated comprehensively. Based on STM, we successfully measure the conductance of a single protein by means of careful control of the feedback system. Compared with previous methods, our improved approach is convenient, and no force induced by the STM tip was applied on the protein when data were being recorded. In our experiments, the structure-dependent electron transport of the single protein, and significant difference in electrical conductivity between α-domain and β-domain structures has been found. In order to prove the reliability of our experimental finding, we also performed the first-principles calculation to simulated molecular orbitals and analyzed the conductance of the β-domain in SOD and α-domain in Hgb, respectively. The results are in great agreement with our experiment data. The mechanisms of the conductivity difference between the α-domain and β-domain have also been explored. This conclusion is extremely valuable for the design of molecular devices. By distinguishing the difference in conductivity of a variety of proteins structures, the direction and intensity of electron transfers in the molecular device can be thoroughly investigated, which greatly improve the predictability in designing the function of the molecular device [41]. Generally speaking, our work should be of important reference value and have great application prospects in some biological fields, including biomolecular electronics and biomolecular nanosensors, etc.

Acknowledgments

References

[1] Aviram A and Ratner M A 1974 Molecular rectifiers *Chem. Phys. Lett.* **29** 277–83

[2] Goldhaber-Gordon D, Montemerlo M S, Love J C, Opiteck G J and Ellenbogen J C 1997 Overview of nanoelectronic devices *P. IEEE* **85** 521–40

[3] Hush N S 2003 An overview of the first half-century of molecular electronics *Ann. NY. Acad. Sci.* **1006** 1–20

[4] Elbing M, Ochs R, Koentopp M, Fischer M, von Hänisch C, Weigend F and Mayor M 2005 Single-molecule diode *PNAS* **102** 8815–20

[5] Del Valle M, Gutiérrez R, Tejedor C and Cuniberti G 2007 Tuning the conductance of a molecular switch *Nat. Nanotechnology* **2** 176–9

[6] Wasielewski M R 1992 Photoinduced electron transfer in supramolecular systems for artificial photosynthesis *Chem. Rev.* **92** 435–61

[7] Bruce A 2007 *Molecular Biology of the Cell* 5th edn (London: Taylor and Francis)

[8] Segal A W 1989 The electron transport chain of the microbicidal oxidase of phagocytic cells and its involvement in the molecular pathology of chronic granulomatous disease *J. Clin. Invest.* **83** 1785–93

[9] Willner I and Katz E 2000 Integration of layered redox proteins and conductive supports for bioelectronic applications *Angew. Chem. Int. Ed.* **39** 1180–218

[10] Uversky V N and Fink A 2007 *Protein Misfolding, Aggregation and Conformational Diseases: B. Molecular Mechanisms of Conformational Diseases* (Berlin: Springer)

[11] Prytkova T R, Kurnikov I V and Beratan D N 2007 Coupling coherence distinguishes structure sensitivity in protein electron transfer *Science* **315** 622–5

[12] Giese B, Graber M and Cordes M 2008 Electron transfer in peptides and proteins *Curr. Opin. Chem. Biol.* **12** 755–9

[13] Skourtis S S and Beratan D N 1999 Theories of structure-function relationships for bridge-mediated electron transfer reactions *Adv. Chem. Phys.* **106** 377

[14] Regan J J and Onuchic J N 1999 Electron-transfer tubes *Adv. Chem. Phys.* **107** 497

[15] Dadosh T, Gordin Y, Krahne R, Khivrich L, Mahalu D, Frydman V, Sperling J, Yacoby A and Bar-joseph L 2005 Measurement of the conductance of single conjugated molecules *Nature* **436** 677–80

[16] James M T 2000 Molecular electronics: synthesis and testing of components *Acc. Chem. Res.* **33** 791–804

[17] Chen F, Hihath J, Huang Z, Li X and Tao N J 2007 Measurement of single-molecule conductance *Annu. Rev. Phys. Chem.* **58** 535–64

[18] Cui X D *et al* 2001 Reproducible measurement of single-molecule conductivity *Science* **294** 571–4

[19] Binnig G and Rohrer H 1983 Scanning tunneling microscopy *Surf. Sci.* **126** 236–44

[20] Xu B and Tao N J 2003 Measurement of single-molecule resistance by repeated formation of molecular junctions *Science* **301** 1221

[21] Xiao X, Xu B and Tao N J 2004 Measurement of single molecule conductance: benzenedithiol and benzenedimethanethiol *Nano Lett.* **4** 267–71

[22] Haiss W, Nichols R J, Zalinge H, Higgins S J, Bethell D and Schiffrin D J 2004 Measurement of single molecule

conductivity using the spontaneous formation of molecular wires *Phys. Chem. Chem. Phys.* **6** 4330–7

[23] Haiss W, Wang C, Grace I, Batsanov A, Schiffrin D J, Higgins S J, Bryce M R, Lambert C J and Nichols R J 2006 Precision control of single-molecule electrical junctions *Nat. Mater.* **5** 995–1002

[24] Scullion L, Doneux T, Bouffier L, Fernig D G, Higgins S J, Bethell D and Nichols R J 2011 Large conductance changes in peptide single molecule junctions controlled by pH *J. Phys. Chem.* C **115** 8361–8

[25] Della Pia E A, Elliott M, Jones D D and Macdonald J E 2012 Orientation-dependent electron transport in a single redox protein *ACS Nano* **6** 355–61

[26] Branden C and Tooze J 1991 *Introduction to Protein Structure* 2nd edn (New York: Garland Publishing)

[27] Leary E, Gonzalez M T, van der Pol C, Bryce M B, Filippone S, Martin N, Rubio-Bollinger G and Agrait N 2011 Unambiguous one-molecule conductance measurements under ambient conditions *Nano Lett.* **11** 2236–41

[28] Meyer E, Hug H J and Bennewitz R 2004 *Scanning Probe Microscopy: the Lab on a Tip* (Berlin: Springer)

[29] Park S and Quate C F 1987 Theories of the feedback and vibration isolation systems for the scanning tunneling microscope *Rev. Sci. Instrum.* **58** 2004–9

[30] Ren B, Picardi G and Pettinger B 2004 Preparation of gold tips suitable for tip-enhanced raman spectroscopy and light emission by electrochemical etching *Rev. Sci. Instrum.* **75** 837–41

[31] Di Ventra M, Pantelides S T and Lang N D 2000 First-principles calculation of transport properties of a molecular device *Phys. Rev. Lett.* **84** 979–82

[32] Xue Y Q, Datta S and Ratner M A 2002 First-principles based matrix Green's function approach to molecular electronic devices: general formalism *Chem. Phys.* **281** 151–70

[33] Taylor J, Guo H and Wang J 2001 *Ab initio* modeling of quantum transport properties of molecular electronic devices *Phys. Rev.* B **63** 245407

[34] Brandbyge M, Mozos J L, Ordejón P, Taylor J and Stokbro K 2002 Density-functional method for nonequilibrium electron transport *Phys. Rev.* B **65** 165401

[35] Xue Y, Datta S and Ratner M A 2001 Charge transfer and 'band lineup' in molecular electronic devices: a chemical and numerical interpretation *J. Chem. Phys.* **115** 4292 1391253

[36] Quek S Y, Venkataraman L, Choi H J, Louie S G, Hybertsen M S and Neaton J B 2007 Amine-gold linked single-molecule circuits: experiment and theory *Nano Lett.* **7** 3477–82

[37] Sepunaru L, Friedman N, Pecht I, Sheves M and Cahen D 2012 Temperature-dependent solid-state electron transport through bacteriorhodopsin: experimental evidence for multiple transport paths through proteins *J. Am. Chem. Soc.* **134** 4169–76

[38] Apsley N and Hughes H P 1975 Temperature and field-dependence of hopping conduction in disordered systems, II. *Philos. Mag* **31** 1327–39

[39] Mott N F 1969 Conduction in non-crystalline materials *Philos. Mag.* **19** 835–52

[40] Fersht A 1999 *Structure and Mechanism in Protein Science: a Guide to Enzyme Catalysis and Protein Folding* (London: Macmillan)

[41] Browne W R and Feringa B L 2006 Making molecular machines work *Nat. Nanotechnology* **1** 25–35